UCL/HEP 99-00?

Study of D^* Production From Virtual Photons at HERA

1^{st} Year Transfer Report

B. West
University College London

Abstract

This report represents a summary of the work undertaken in the 1^{st} year of my Ph.D.. Presented is an observation of D^* production from a virtual photon at the ZEUS detector. The ZEUS Beam Pipe Calorimeter was used to measure positrons scattered through small angles (15 - 34 mrad) and tagged a sample of events with photon virtualities in the range 0.1 GeV^2 $<$ Q^2 $<$ 0.65 GeV^2.

Submitted for the transfer from M. Phil. to Ph. D. status.

1 Introduction

The partonic structure of the quasi-real photon is well established and has been studied at both e^+e^- colliders (in two-photon interactions) [1] and HERA (in jet photoproduction) [2]. In photoproduction processes at HERA, a quasi-real photon ($Q^2 \approx 0$) is emitted by the incoming electron or positron, and interacts with the proton. At leading order (LO) in QCD, two types of process take part: direct, where the photon couples as a point-like particle to a parton from the proton, and resolved, where one of the partons in the photon scatters on a parton in the proton. Studies of dijet photoproduction at HERA have shown that both processes are present for quasi-real photons [2]. At present, however, there is very little experimental information on the partonic structure of virtual photons. For a long time the only published data were from PLUTO [3] and hampered by low statistics. e^+e^- colliders can only study virtual photons in double-tag events, resulting in very low statistics [4]. HERA is then in the unique position of being able to study photons over a wide range of virtualities, Q^2, from photoproduction to high Q^2 deep inelastic scattering whilst being sensitive to any photon structure.

Theoretical studies [5] predict that for dijet cross-sections the resolved contribution should decrease relative to the direct contribution (*i.e.* the partonic content of the photon is suppressed) as Q^2 increases. Specifically, for virtual photons, the Vector Meson Dominance (VMD) component of the resolved photon is predicted to decrease as $\sim (m_v^2/(m_v^2 + Q^2))^2$, while the perturbative QCD (pQCD) component is predicted to decrease more slowly, as $\sim ln({E_T^{jet}}^2/Q^2)$. Recently, H1 has studied the transition between photoproduction and deep inelastic scattering by measuring the inclusive jet and dijet cross-sections in the $\gamma^* p$ frame [6] and ZEUS has studied the Q^2 dependence of the photon structure by measuring the ratio of direct to resolved dijet cross sections as a function of Q^2 [7]. Both studies were consistent with the predicted suppression of the partonic component of the photon with Q^2.

In this analysis we present a study of the charm structure of the virtual photon using a sample of low Q^2 tagged events collected at the ZEUS detector. If, as we might intuitively guess, the charm structure of the resolved photon arises predominantly from the pQCD component with little or no VMD contribution, then the resolved component should decrease more slowly than has been observed for light quarks. Furthermore the large charm mass should make calculations of the pQCD component more reliable than those for light quarks. Therefore, measurements of the Q^2 evolution of the resolved charm photon component are expected to test perturbative QCD.

Charm was tagged by identifying $D^{*\pm}(2010)$ mesons in the final state via the charged products of their decay. D^* mesons were reconstructed through the decay channel[1]:

$$D^{*+} \to D^0 \pi_s^+ \to (K^- \pi^+) \pi_s^+. \tag{1}$$

The small mass difference $\Delta m = m(D^*) - m(D^0) = 145.40 \pm 0.03$ MeV [8] yields a low momentum ("soft") pion, π_s, from the D^* decay and a prominent signal just above the threshold of the Δm distribution, where the light flavour combinatorial background is highly restricted by phase space.

[1]Hereafter $D^{*\pm}(2010)$ are referred to as D^* and the charge conjugate processes are also included.

2 Event Kinematics

Neutral Current ep scattering $e(k)+p(P) \to e(k')+X$ can be described with the following kinematic variables:

$$\sqrt{s} = \sqrt{(k+P)^2} \approx \sqrt{4E_pE_e} = 296 \text{ GeV}, \tag{2}$$

the total ep centre of mass energy;

$$q^2 = -Q^2 = (k-k')^2, \tag{3}$$

the four-momentum transfer squared carried by the virtual photon;

$$y = \frac{q \cdot P}{k \cdot P}, \tag{4}$$

the Bjorken variable describing the energy transfer to the hadronic system; and

$$W^2 = (q+P)^2 = -Q^2 + ys + m_p^2, \tag{5}$$

the centre of mass energy squared of the γp system, where m_p is the mass of the proton.

The variable y can be determined to a good approximation from the hadronic system using the Jacquet-Blondel expression:

$$y_{\mathrm{JB}} = \frac{\sum_i (E_i - p_{z,i})}{2E_e}, \tag{6}$$

with the sum running over all calorimeter cells except those associated with the scattered electron.

If the scattered electron is seen in the detector, the variable y can also be obtained from[2]:

$$y_e = 1 - \frac{E'_e}{2E_e} \cdot (1 - cos\theta'_e). \tag{7}$$

3 The ZEUS Detector

A detailed description of the ZEUS detector can be found in refs. [9, 10]. Here we present a brief description of the components relevant to the present analysis.

3.1 The Central Tracking Detector (CTD)

Charged particles were measured by the CTD [11] which operates in a magnetic field of 1.43 T provided by a thin superconducting solenoid. The CTD is a drift chamber consisting of 72 cylindrical layers, arranged in 9 superlayers covering the polar angle region $15° < \theta < 164°$. The nominal CTD resolution for long (superlayer > 3) tracks is 180 - 190 μm in r - ϕ and $(\sigma_{p_T}/p_T)^{track} = 0.005 p_T^{track} \oplus 0.016$ (p_T^{track} in GeV). The CTD was also used to establish an interaction vertex for each event.

[2]We use the standard ZEUS right-handed coordinate system in which the positive z-axis points in the direction of the proton beam and the positive x-axis points towards the centre of HERA with the origin at the nominal interaction point.

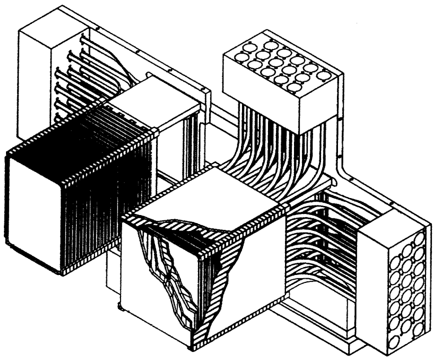

Figure 1: *The BPC north and south modules.*

3.2 The Uranium Calorimeter (CAL)

Surrounding the solenoid is a uranium-scintillator sampling calorimeter [12], which is divided into three sections, the FCAL in the forward direction, RCAL in the rear and BCAL in the barrel region surrounding the CTD. The CAL is hermetic and consists of 5918 cells each read out by two photomultiplier tubes. The energy resolution of the CAL measured under test beam conditions has been found to be $0.18/\sqrt{E}$ for electrons and $0.35/\sqrt{E}$ for hadrons (E in GeV).

3.3 The Beam Pipe Calorimeter (BPC)

The BPC [13], shown in Figure 1, is a tungsten-scintillator sampling calorimeter which sits around the beampipe, within the RCAL and provides position and energy measurements of DIS electrons at very small scattering angles. The BPC consists of two modules, north and south, installed approximately -293.7 cm from the nominal interaction point at a distance of 4 cm and 8 cm with respect to the HERA beams. The energy resolution of the BPC is $0.17/sqrt(E_e')$ and the position resolution is 0.5 mm resulting in a Q^2 resolution of 6%.

4 Definition of the Cross-section

The kinematic region for the measurement presented in this report is defined by the following:

$$0.2 < y < 0.55,$$

$$0.1 \text{ GeV}^2 < Q^2 < 0.55 \text{ GeV}^2,$$

$$p_T(D^*) > 3 \text{ GeV},$$

$$|\eta(D^*)| < 1.5.$$

The Q^2 and y intervals were constrained by the acceptance of the BPC. The y interval corresponds to a γp centre-of-mass energy, $W_{\gamma p} \approx \sqrt{y.s}$ of 134 GeV $< W <$ 223 GeV. The $p_T(D^*)$ cut was chosen to be this high as this provided a cleaner signal than a lower cut. The pseudorapidity cut ensured that all tracks forming the D^* were well reconstructed in the CTD.

5 Data Selection and Trigger

For this analysis data from the 1996 and 1997 running periods were used, corresponding to an integrated luminosity of 38.1pb^{-1}. The data selection procedure took place in two parts - the online selection, involving the first and second level hardware triggers and a third level software trigger, and the offline selection which took advantage of the fully reprocessed data.

5.1 Online Data Selection

The online selection required that an event pass slot 42 at the first level trigger, slot HPP01 at the second level trigger and slot HFL10 at the third level trigger.

5.1.1 First Level Trigger (FLT)

At the FLT a short decision time was necessary, with only limited detector information available. As a result, FLT cuts were on simple detector properties such as global or regional energy sums, simple tracking requirements and vetoes. For an event to have passed slot 42 at the FLT five vetoes, a track quality demand and one of four Calorimeter FLT (CFLT) thresholds must have been satisfied.

- The veto criteria were:
  - The timings observed in the two C5 counters should have matched with physics timing, but not with beam-gas timing.
  - The timings observed in the SRTD should have matched with physics timing, but not with beam-gas timing.
  - The CTD-FLT should have allocated TRKclass>2 based upon the multiplicity of all tracks and vertex tracks.
  - The remaining two vetoes required that there be no coincidence in the inner and outer layers of the vetowall.
- The track quality demand required that the CTD-FLT found at least one track coming from the nominal interaction region, -50 cm $< z_{vtx}^{FLT} <$ 80 cm.

- The CFLT thresholds were:
  - total calorimeter energy > 14.968 GeV;
  - total ElectroMagnetic Calorimeter (EMC) Energy > 10.068 GeV;
  - RCAL EMC energy > 2.032 GeV;
  - BCAL EMC energy > 3.404 GeV.

  The calculation of these energies excluded the 3 inner rings around the FCAL and the inner ring around the RCAL beampipe.

5.1.2 Second Level Trigger (SLT)

At the SLT more time was available, so the triggers were able to use more sophisticated algorithms and more complete detector information than was available at the FLT. This meant cuts on physical quantities such as $E-P_z$ could be introduced and the vertex could be determined more accurately. For an event to have passed slot HPP01, designed for general purpose hard photoproduction, several high transverse energy requirements must have been satisfied:

- -60 cm $< z_{vtx}^{SLT} <$ 60 cm;
- at least 1 track was associated with the vertex (this is identical to the track condition at the FLT);
- $E - P_z > 8.0$ GeV;
- $E_T(box) > 8.0$ GeV, where $E_T(box)$ is the sum of transverse energy over all calorimeter cells excluding the first ring around the FCAL beampipe;
- either ($E - P_z > 12.0$ GeV) or ($p_z/E < 0.95$).

5.1.3 Third Level Trigger (SLT)

At the TLT the full event information was available. Slot HFL10, designed to trigger on $D^* \rightarrow k\pi\pi_s$ decays, used a stripped down version of the full offline tracking to reconstruct D^*s. The reconstruction method used here was identical to that in this analysis, described in section 6, with the following (looser) cuts:

$$p_T(K,\pi) > 0.4 \text{ GeV},$$

$$p_T(\pi_s) > 0.1 \text{ GeV},$$

$$1.4 \text{ GeV} < m(D^0) < 2.2 \text{ GeV},$$

$$p_T(D^*) > 1.8 \text{ GeV},$$

$$\Delta\mathrm{M} < 0.175 \text{ GeV},$$

$$\Delta\mathrm{M} < 0.165 \text{ GeV or } m(D^0) > 1.65 \text{ GeV}.$$

5.2 Offline Data Selection

The event sample was processed using the standard offline ZEUS detector calibration and event reconstruction code. Several corrections were then applied to calorimeter quantities before further cuts were applied:

- Channels which gave large energy readings irrespective of hadronic activity in the cell were removed. This removed "hot" cells in which the activity was due to electronics malfunctions.
- A cut on relative cell imbalance was applied and isolated EMC and HAC cells with energies below 80 and 140 MeV respectively were removed. This removed cells in which the activity was due to background radiation from the calorimeter and noise in the electronics.
- To correct for differences between data and Monte Carlo an energy scale correction of 1.05 and 1.025 was applied to BCAL and RCAL cells respectively.

5.2.1 Photoproduction Selection

To define an inclusive photoproduction sample, the following requirements were imposed:

- No scattered positron found in the CAL by the `SINISTRA` [14] algorithm, with probability > 0.9 satisfying $E'_e > 5$ GeV and $y_e < 0.7$. This requirement removes neutral current DIS events.
- $0.15 < y_{\mathrm{JB}} < 0.45$. The upper cut rejects DIS events in which the scattered electron had not recognised by `SINISTRA`. In this case the scattered electron would have been included in the calculation of y_{JB} with the result that $E - p_z \to 2E_e$ and $y_{\mathrm{JB}} \to 1$. The lower cut rejects beam-gas events and also rejects events from a region in which the acceptance is small due to trigger requirements. Beam-gas events are characterised by low values of y_{JB} because $E - p_z$ is a measure of E'_e which, for a (proton) beam-gas interaction, will be zero.

5.2.2 BPC Selection

The south BPC module is used primarily for calibration purposes and was excluded from this analysis. BPC quantities were reconstructed using the BPRECON [15] routine and the following cuts were applied:

- A fiducial volume cut, shown in figure 2a, was applied to ensure that the electron was fully contained in the active region of the BPC.

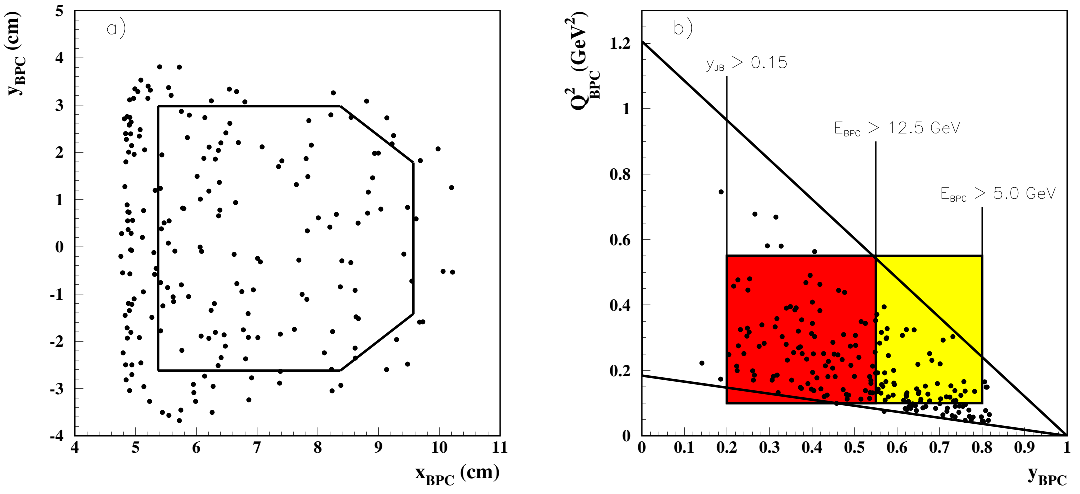

Figure 2: *a) BPC fiducial volume cuts. b) BPC acceptance. The solid boxes show the kinematic region measured by the standard and loose selection criteria. The triangular region is the physical acceptance of the BPC.*

- $E'_e > 12.5$ GeV. This is effectively a y_e cut and confines us to a region of (y, Q^2) space, shown in figure 2, in which we have almost complete acceptance. When comparing data and Monte Carlo and studying dijet events it was necessary to increase the statistics of the sample. Modified cuts[3] of $E'_e > 5$ GeV and $0.15 < y_{\rm JB} < 0.7$ were used resulting in a doubling of the event sample.

6 D^* Reconstruction

D^* candidates were identified by combining all permutations of three tracks (K, π, π_s candidates) such that they pass certain criteria. Only tracks associated with the event vertex, having $p_T^{track} > 0.2$ GeV and hits out to at least superlayer 3 of the CTD were included in the combinations. All pairs of tracks with opposite charge and,

$$p_T(K, \pi) > 0.5 \text{ GeV},$$

were combined to form D^0 candidates. Since no particle identification was used, kaon and pion masses were assigned to both particles in turn. The D^0 candidate formed from these tracks was kept if the reconstructed mass was in the range,

$$1.6 \text{ GeV} < m(D^0) < 2.2 \text{ GeV}.$$

The surviving D^0 candidates were then combined with a third track, having opposite charge to the kaon candidate, to form a D^* candidate. This candidate was accepted if it

[3]Hereafter referred to as the loose selection criteria.

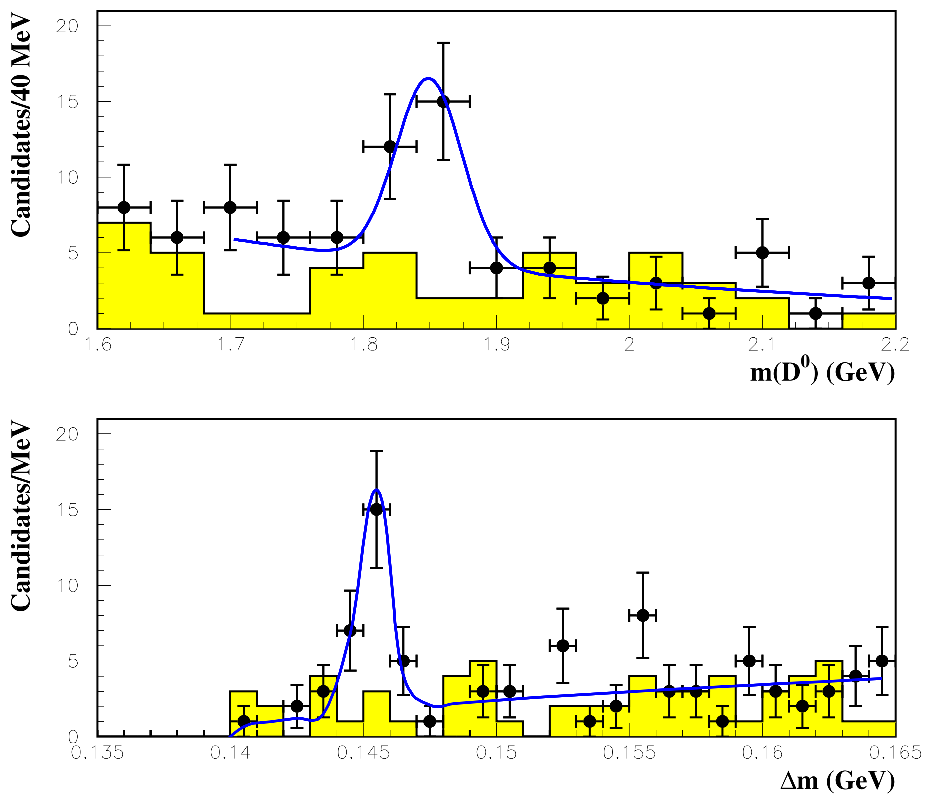

Figure 3: *1996-7 mass signals for BPC events passing the loose data selection criteria with the additional demand of jets. The solid histogram shows the wrong charge background estimate and the solid line the fitted function.*

satisfied the following;

$$p_T(D^*) > 3 \text{ GeV},$$

$$|\eta(D^*)| < 1.5,$$

$$0.135 \text{ GeV} < \Delta\text{M} < 0.165 \text{ GeV}.$$

6.1 Signal Mass Distributions

The mass windows used up to this point are wide and lead to very large backgrounds. In order to study the mass signals it was necessary to use tighter mass windows. For the analysis of the Δm distribution a cut around the central value of the mass of the D^0 meson, 1864.5 $\pm$ 0.05 MeV [8], was made:

$$1.80 \text{ GeV} < m(D^0) < 1.92 \text{ GeV}.$$

Similarly a cut around the central value of the mass difference, 145.42 $\pm$ 0.05 MeV [8], was made for the analysis of the $m(D^0)$ distribution:

$$0.143 \text{ GeV} < \Delta m < 0.148 \text{ GeV}.$$

Clear signals were observed in both distributions, shown in figure 3. In the absence of any background the signal would be Gaussian. However, since a combinatorial background will also have passed the selection cuts the distribution is described by a Gaussian plus some background function. The mass difference background was described by $A(x - m_\pi)^B$ and the D^0 background by Ae^{-Bx}. In both cases A and B were determined from the fit to the signal using a maximum likelihood method. In common with previous analyses [18] the $m(D^0)$ fit excluded low values of $M(D^0)$. This was done to exclude the effects of another resonance in which the D^0 meson decays to a kaon, pion and π^0. The π^0 leaves no track and so does not enter into the calculation, resulting in a lower invariant mass for the reconstructed D^0 meson. Here the effect is masked by the limited statistics. The fitted functions, shown in figure 3, describe well what is seen and give the following results for the masses;

$$\Delta m = 145.35 \pm 0.18 \text{ MeV},$$

$$m(D^0) = 1849.4 \pm 8.6 \text{ MeV}.$$

The value for the mass difference is in good agreement with the value given by the particle data group [8]; $\Delta m = 145.40 \pm 0.03$ MeV. The mass of the D^0 is lower than the nominal value; $m(D^0) = 1864.6 \pm 0.5$ MeV. This is consistent with a systematic uncertainty in the magnetic field of the CTD and does not effect the results of this analysis.

6.2 Background Estimation

Previous D^* analyses have estimated the background under the signal using two independent methods:

- Wrong charge - combinations in which the tracks forming the D^0 candidate have the same charge, all other criteria remaining the same, are used.
- Control region - events which lie outside (but close to) the signal region of the mass distributions are used.

Due to the limited statistics in the present analysis, both methods are highly sensitive to statistical fluctuations in the background distribution. As a result no background subtraction was attempted, instead the number of D^* events in the signal was estimated using unbinned maximum likelihood fits, as outlined in ref. [16]. The number of D^* events satisfying the loose cuts was estimated from the fit to the mass difference and found to be 22 $\pm$ 6 D^* mesons. This was in good agreement with 19 $\pm$ 6, from the D^0 distribution and 19 $\pm$ 8, using wrong charge subtraction.

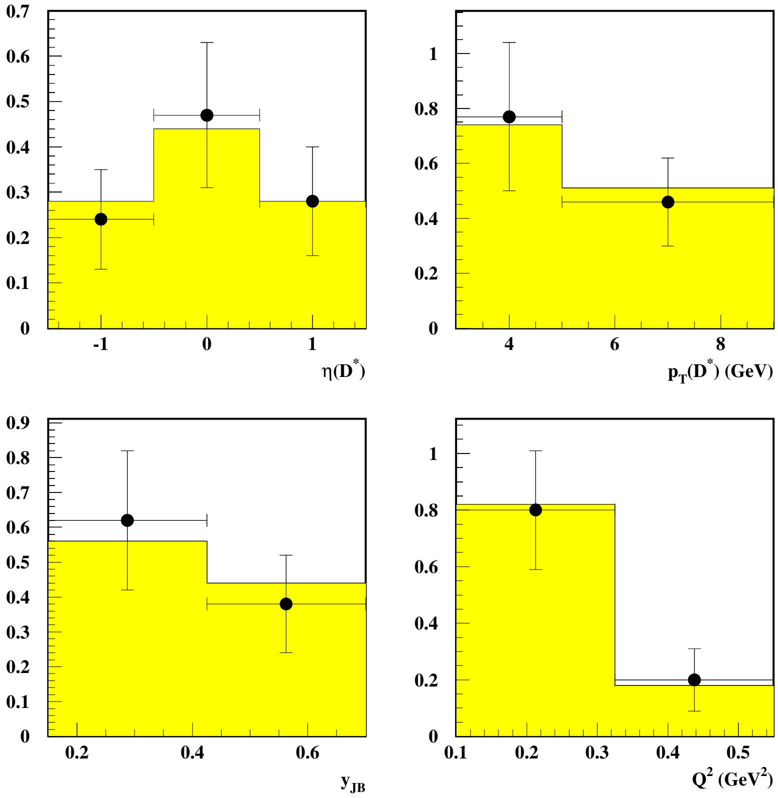

Figure 4: *Comparison of data (solid points) with Monte Carlo (histograms) for events passing the loose data selection criteria.*

7 Monte Carlo Simulation

7.1 Monte Carlo Overview

Large, general purpose detectors such as ZEUS, are highly complex and measurements of cross-sections must be corrected for the effects of finite detector resolutions, efficiency and acceptance. The Monte Carlo program HERWIG 5.9 [17] was used to model the hadronic final states in charm production. Events containing at least one D^* decaying to $K\pi\pi_s$ were processed through the standard ZEUS detector and trigger simulation programs and through the event reconstruction package used for offline data processing. The sample used was the same as that used in ref. [18] and is described in more detail therein.

7.2 Comparison of Data and Monte Carlo

The correction of data using the ratio of generated to reconstructed Monte Carlo events is only valid when the Monte Carlo correctly describes the data distributions of quantities used in the analysis. Figure 4 shows the comparison of quantities between data and Monte

Carlo. The two are area normalised to unity, so no relevance should be drawn from the y-axis and only a shape comparison should be made. All quantities show reasonable agreement between the data and Monte Carlo.

8 Correction to the Cross-section

The total cross-section σ was obtained using the expression:

$$\sigma = \frac{N}{\int \mathcal{L}dt.\mathrm{BR.Acc}}, \tag{8}$$

where BR is the branching ratio of the process $D^* \to K\pi\pi_s$ (0.0263 ± 0.0008 [8]), N is the number of events observed, $\int \mathcal{L}dt$ is the integrated luminosity ($\int \mathcal{L}dt = 38.1$ nb) and Acc is the acceptance, defined by

$$Acc = \frac{R}{T}. \tag{9}$$

R is the number of reconstructed events which pass the data selection criteria. T is the number of "true" hadronic events passing the selection criteria of the cross-section definition in section 4. The overall acceptance in this kinematic region defined was found to be 2.4%.

Using the above quantities we measure an ep cross-section for D^* photoproduction, of:

$$\sigma_{ep \to D^* X} = 0.50 \pm 0.19 \text{ nb},$$

in the kinematic region $0.2 < y < 0.55$ and $0.1 < Q^2 < 0.55$, $p_T(D^*) > 3$ GeV, $|\eta(D^*)| < 1.5$. Only statistical errors have been presented here.

9 Resolved Charm in the Virtual Photon

The measurement of jets in the final state allows the kinematics of the hard scattering process to be reconstructed. In order to define a dijet sample the following requirements were imposed on the two highest energy jets;

$$E_T^{jet} > 4 \text{ GeV},$$

$$|\eta^{jet}| < 2.4.$$

Using these jets we define;

$$x_\gamma^{obs} = \frac{\sum_{jets}(E_T^{jet} e^{-\eta^{jet}})}{2E_e y}, \tag{10}$$

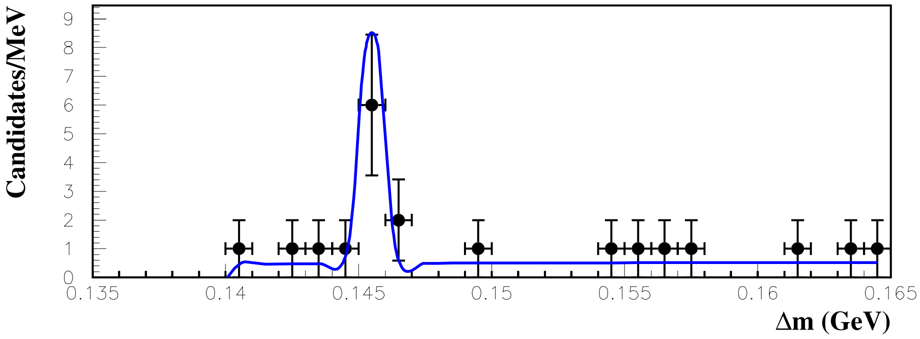

Figure 5: *1996-7 Δm mass signal for resolved ($x_\gamma^{obs} < 0.75$) dijet events passing the loose data selection criteria.*

where η^{jet} is the jet pseudorapidity, y is estimated by $y_{\rm JB}$, and the jets in the sum are the two highest E_T^{jet} jets within the accepted η^{jet} range. The variable x_γ^{obs} is the fraction of the photon momentum contributing to the production of the two jets with the highest E_T^{jet}. In measurements as well as in Monte Carlo simulations and higher order calculations, direct and resolved samples can be separated by a cut on x_γ^{obs}. In this analysis we define a resolved photon process by the selection $x_\gamma^{obs} < 0.75$.

The Δm signal for resolved events passing the loose selection cuts is shown in figure 5. A clear peak at the nominal value of Δm is evident. The number of events estimated from the fit is 7 ± 3.

10 Conclusions and Discussion

We have observed 22 D^* mesons in the decay channel $D^* \to K\pi\pi_s$ in $\gamma^* p$ interactions at HERA. The ep cross-section for inclusive D^* production for events with $0.1 < Q^2 < 0.55$ and $0.2 < y < 0.55$ was found to be 0.5 ± 0.19 nb in the restricted kinematic region $p_T(D^*) > 3$ GeV and $|\eta(D^*)| < 1.5$.

A signal for the production of D^* mesons from resolved photons with a virtuality in the range 0.1 GeV^2 $< Q^2 <$ 0.55 GeV^2 has been observed. Present statistics, however, were too low for a measurement of the resolved charm component of the virtual photon.

After 2000, upgrades to the ZEUS detector, together with HERA's promised increase in luminosity, should allow studies with far higher statistics to be made. Unfortunately, these upgrades will require the removal of the BPC, so the measurement presented here will not benefit. However, the proposed microvertex detector for ZEUS [19] will enable more efficient methods of charm tagging, such as the detection of secondary vertices, to be used so similar measurements using low Q^2 DIS events will still be possible.

References

[1] M. Drees and R. Godbole, hep-ph 9508221, (1995);
T. Sjöstrand, J. Storrow, A. Vogt, hep-ph 9601351, (1996).

[2] Zeus Collaboration, M. derrick et al., Phys. Lett. **B322** (1994) 287;
Zeus Collaboration, M. derrick et al., Phys. Lett. **B348** (1995) 665;
Zeus Collaboration, M. derrick et al., Eur. Phys J. **C1** (1998) 109;
H1 Collaboration, T. Ahmed et al., Phys. Lett. **B297** (1992) 205;
H1 Collaboration, I. Abt et al., Phys. Lett. **B314** (1993) 436;
H1 Collaboration, C. Adloff et al., Eur. Phys. J. **C1** (1998) 97.

[3] Pluto Collaboration, C. Berger et al., Phys. Lett. **B142** (1984) 119.

[4] N. Zimin, Prospective Results at Very Low Q^2 at LEP2, Proceedings of Workshop on Photon Interactions and the Photon Structure, Lund, Sweden, p117-124, 10-13 Sep. 1998.

[5] M. Klasen et al., hep-ph/9703302 (1997).

[6] H1 Collaboration, Measurement of Dijet Cross-Sections at low Q^2 and the Extraction of an Effective Parton Density for the Virtual Photon, DESY 98-205, submitted to Eur. Phys. J. C.

[7] Zeus Collaboration, M. Derrick et al., Dijet Cross Sections in γp Interactions Using Real and Virtual Photons at HERA, not yet published.

[8] C. Caso et al., Particle Data Group, Eur. Phys. J. **C3** (1998).

[9] ZEUS Collaboration, M. Derrick et al., Phys. Lett. **B293** (1992) 465.

[10] ZEUS Collaboration, M. Derrick et al., The ZEUS Detector Status Report 1993, DESY 1993.

[11] N Harnew et al., Nucl. Instr. Meth. **A279** (1989) 290;
B. Foster et al., Nucl. Phys. B (Proc. Suppl.) **32** (1993) 181;
B. Foster et al., Nucl. Instr. Meth. **A338** (1994) 254.

[12] M Derrick et al., Nucl. Instr. Meth. **A309** (1991) 77;
A. Anderson et al., ibid. **A309** (1991) 101;
A. Caldwell et al., ibid. **A321** (1992) 356;
A. Bernstein et al., ibid. **A336** (1993) 23.

[13] A. Caldwell et al., On the New Beam Pipe Calorimeter, ZEUS Note 94-129;
J. Breitweg et al., Phys. Lett. **B407** (1997) 432-448.

[14] ZEUS Collaboration, M. Derrick et al., Phys. Lett. **B322** (1994) 287.

[15] U. Fricke, BPRECON - User's Guide and Reference, ZEUS Note 98-081.

[16] P. Nylander, A Systematic Method for Unbinned Fitting and Statistical Analysis, ZEUS Note 97-096.

[17] G Marchesini et al., Comp. Phys. Comm. **67** (1992) 465.

[18] ZEUS Collaboration, M. Derrick et al., Eur. Phys. J. **C6** (1999) 67.

[19] The ZEUS Collaboration, A Microvertex Detector for ZEUS, ZEUS Note 97-006.